Electronic Supplementary Information

From Ru nanoparticle-encapsulated metal-organic framework to highly catalytically active Cu/Ru nanoparticle-embedded porous carbon

Pradip Pachfule,[a] Xinchun Yang,[a,b] Qi-Long Zhu,[a] Nobuko Tsumori,[c] Takeyuki Uchida,[a] and Qiang Xu*[a,b]

[a.] *National Institute of Advanced Industrial Science and Technology (AIST), Ikeda, Osaka 563-8577, Japan. Fax: +81-72-751-9629; Tel: +81-72-751-9562. *E-mail: q.xu@aist.go.jp*

[b.] *Graduate School of Engineering, Kobe University, Nada Ku, Kobe, Hyogo 657-8501, Japan.*

[c.] *Toyama National College of Technology, Hongo-machi, Toyama 939-8630, Japan.*

Contents

Section S1. General instrumentation and methods

Powder X-ray diffraction (PXRD) measurements were performed on a Rigaku Ultima IV X-ray diffractometer with a Cu Kα source. Raman scattering spectra were recorded on a laser Raman microscope system (Nanophoton RAMANtouch) with an excitation wavelength of 532 nm. Thermo-gravimetric analyses (TGA) were carried out on a Rigaku Thermo plus EVO2/TG-DTA analyzer under argon atmosphere at a heating rate of 5 °C min^{-1} within the temperature range of 25–800 °C. Fourier transform infrared spectroscopy (FTIR) analyses were carried out on Shimadzu IRTracer-100 using ATR mode. The metal contents of the MOF and carbon samples were analyzed using ICP-OES on Thermo Scientific iCAP6300. X-ray photoelectron spectroscopic (XPS) measurements were conducted on a Shimadzu ESCA-3400 X-ray photoelectron spectrometer using a Mg Kα source (10 kV, 10 mA). N_2 sorption measurements were performed on a volumetric sorption instrument (BELSORP-Max). Prior to the gas sorption measurements, the samples were dried under a dynamic vacuum (<10^{-3} Torr) at room temperature followed by heating at 80 °C for 12 h and 150 °C for 12 h. Using N_2 sorption isotherms, the surface areas were calculated by applying Brunauer-Emmett-Teller (BET) method and the pore size distributions were calculated using the non-localized density functional theory (NLDFT) method. Scanning electron microscopy (SEM) analyses were performed on Hitachi S5000 and JEOL JSM-IT100. Transmission electron microscopy (TEM), high-angle annular dark field scanning transmission electron microscopy (HAADF-STEM), electron tomographic measurements and selected area electron diffraction (SAED) analyses for the detailed microstructure and composition information were executed on FEI TECNAI G^2 F20 at an accelerating voltage of 200 kV.

Section S2. Experimental section

Durability test of catalysts: After the completion of a run of AB hydrolysis reaction, another aliquot of AB solution (1 mmol in 1 mL water) was added into the reaction system and the released gas was monitored by the gas burette. 5 runs of such catalytic reactions were carried out at room temperature. After hydrolysis reaction, the spent catalysts were separated from the reaction solution by centrifugation and dried under vacuum at room temperature, which were used for PXRD and TEM analyses.

Also, the recyclability test for the hydrogen generation from aqueous AB solution has been carried out by isolating the Cu/Ru@C-1b catalyst after each successive cycle. After the successive cycle, the spent catalysts was separated from the reaction solution by centrifugation, washed and dried under vacuum at room temperature, which was further used to analyze the recyclability of the catalyst. 4 runs of such catalytic reactions were carried out at room temperature.

Calculation Methods: The TOF reported here is an apparent TOF value calculated based on the number of Ru atoms in catalyst (Cu/Ru@C-1a, -1b and -1c) and the time of half-completion of gas generation[1] according to following equation:

$$\mathrm{TOF} = \frac{P_{\mathrm{atm}} V_{\mathrm{gas}} / RT}{n_{\mathrm{Ru}} t}$$

where P_{atm} is the atmospheric pressure (101325 Pa), V_{gas} is the generated volume of H_2 gas at the time of half-completion of gas generation, R is the universal gas constant (8.3145 m^3 Pa mol^{-1} K^{-1}), T is the room temperature (298 K), n_M is the total mole number of Ru atoms in catalyst, and t is the time of half-completion of gas generation. The TOF values have been calculated based on the amount of ruthenium in Cu/Ru@C-1a, -1b and -1c, because the ruthenium is the active component of the catalysts.

Table S1. Summary of starting materials used for synthesis and porosity details of MOF and MOF composites.

MOF	$Cu(NO_3)_2 \cdot 3H_2O$ (mmol)	$RuCl_3 \cdot xH_2O$ (mmol)	BTC (mmol)	Surface area ($m^2\ g^{-1}$)	Pore Volume ($cm^3\ g^{-1}$)
HKUST-1	4.84	-	2.34	1762	1.407
Ru@HKUST-1a	3.87	0.97	2.34	892	0.793
Ru@HKUST-1b	4.11	0.73	2.34	1094	0.977
Ru@HKUST-1c	4.35	0.49	2.34	1467	1.178

Table S2. Summary of ICP analyses and catalytic activities.

Sample	Cu (wt.%)	Ru (wt.%)	Turnover frequency (TOF) for H_2 generation ($mol_{H2} \cdot mol_{cat}^{-1} \cdot min^{-1}$) at 298 K[a]
Ru@HKUST-1b	21.2	3.4	-
Cu@C	83.3	0.0	-
Cu/Ru@C-1a	67.0	17.7	46
Cu/Ru@C-1b	67.8	9.4	97
Cu/Ru@C-1c	70.6	4.7	56

[a] *TOF based on Ru amount and the time of half completion of gas generation.*

Section S3. Characterization of MOF and carbon composites

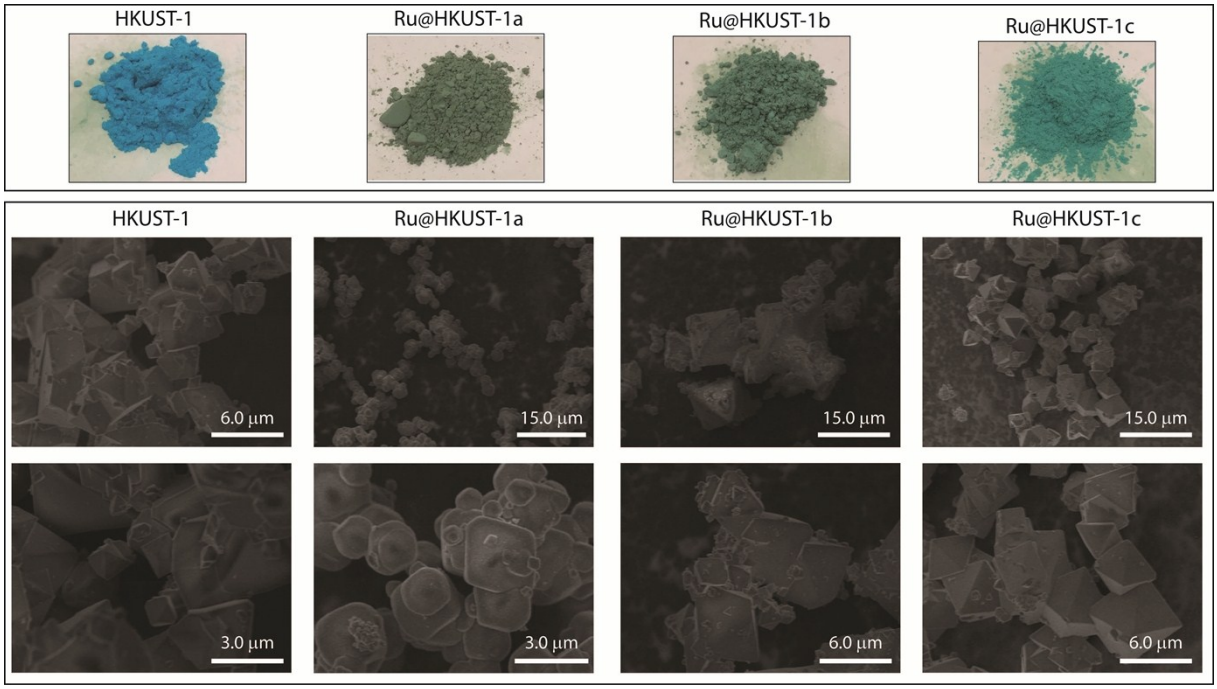

Fig. S1 Optical and SEM images of HKUST-1, Ru@HKUST-1a, -1b and -1c, showing the formation of microcrystalline MOF particles with octahedral morphologies.

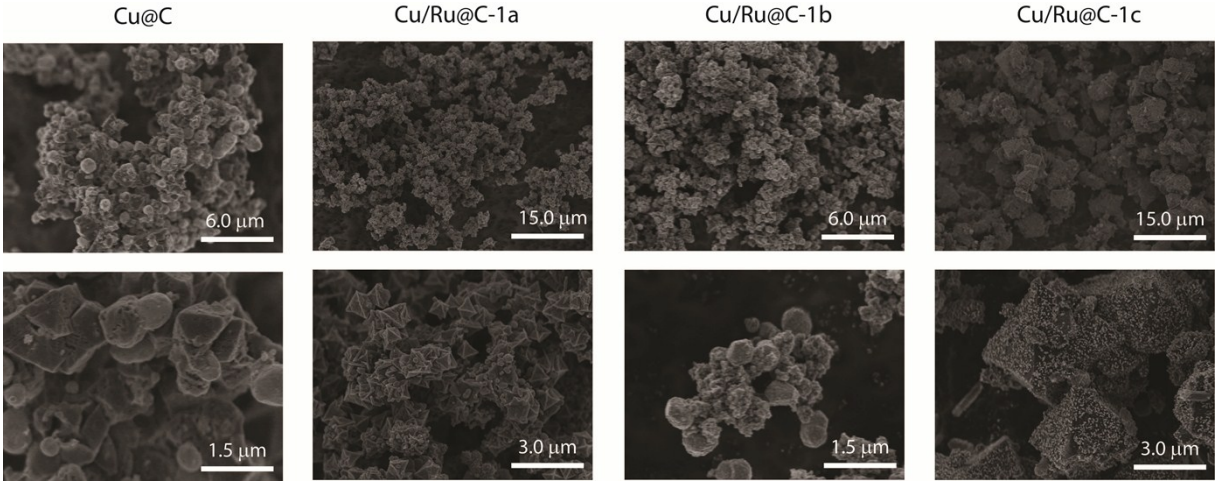

Fig. S2 SEM images of Cu@C, Cu/Ru@C-1a, -1b and -1c synthesized through the morphology-preserved thermal transformation of HKUST-1, Ru@HKUST-1a, -1b and -1c, respectively, showing the maintenance of parent octahedral morphology in carbon composites.

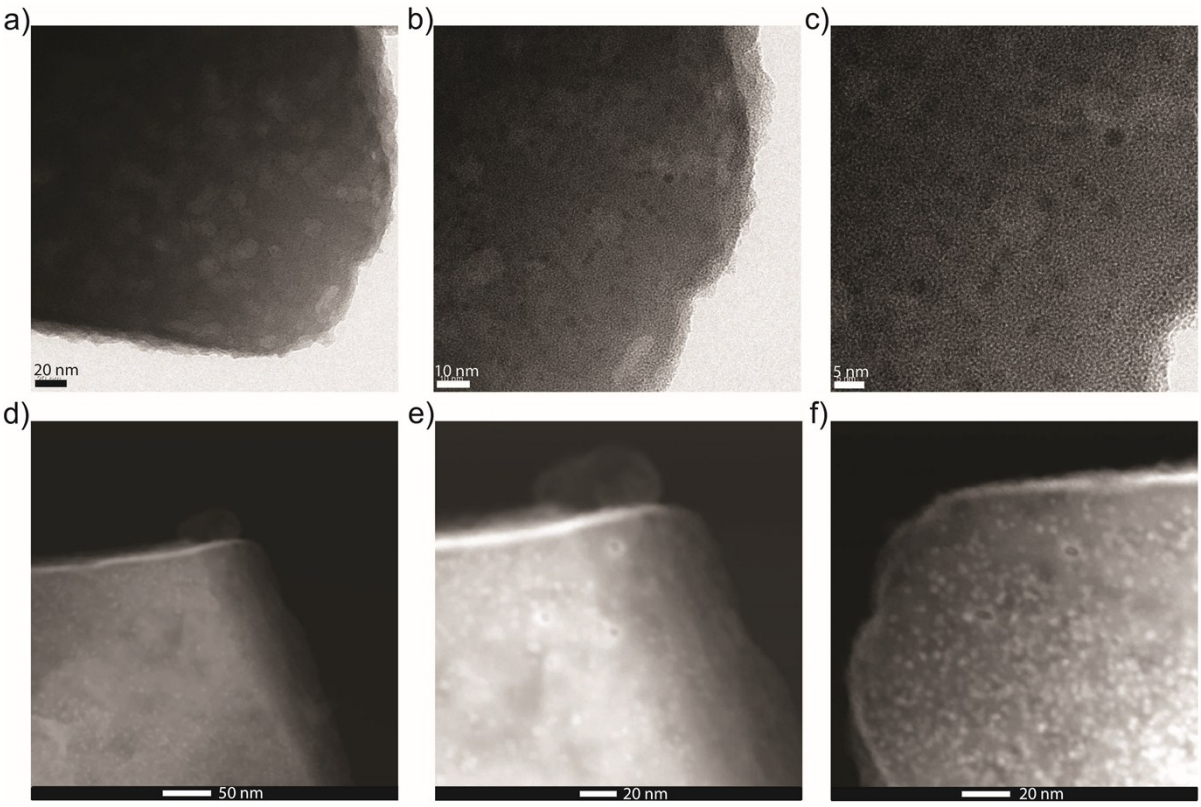

Fig. S3 (a) Low-magnification TEM, and (b, c) HRTEM images of Ru@HKUST-1b, showing the encapsulation of highly dispersed Ru nanoparticles in MOF matrix. (d) Low-magnification HAADF-STEM and (e, f) high-magnification HAADF-STEM images of Ru@HKUST-1b, showing the mono-dispersed Ru nanoparticles throughout the Ru@HKUST-1b crystals.

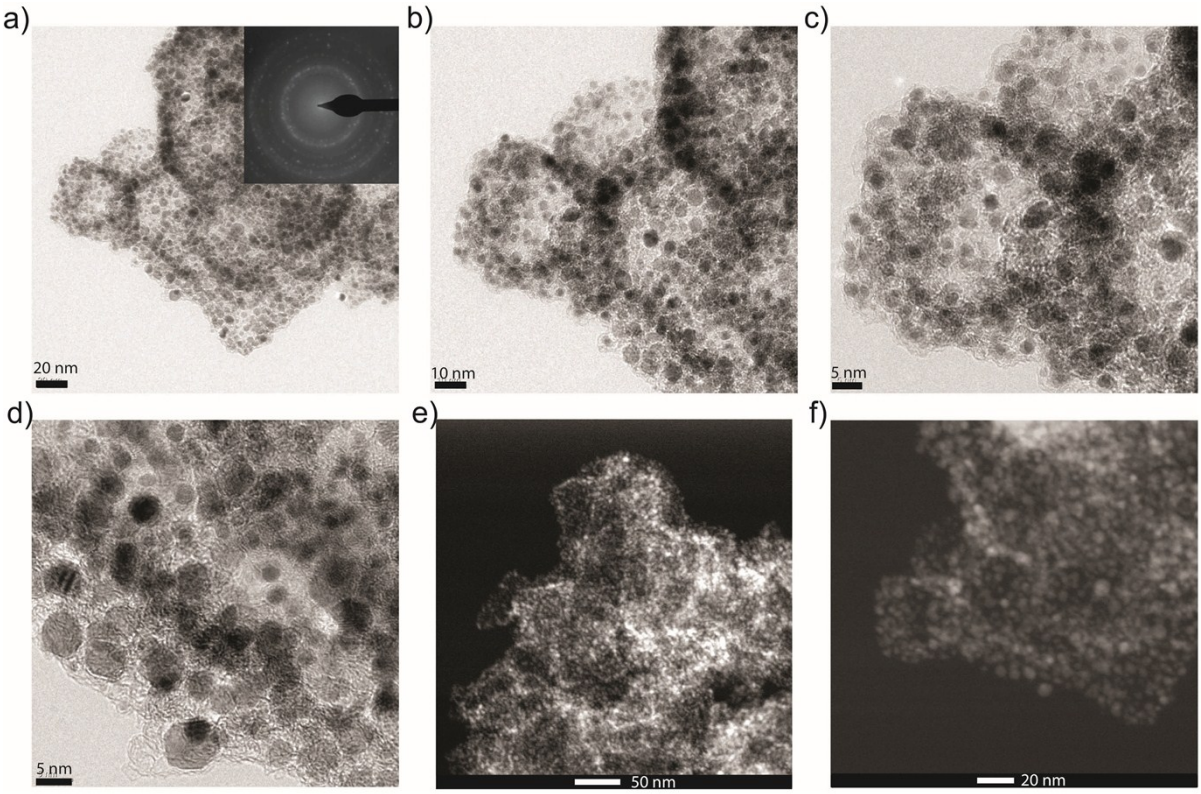

Fig. S4 (a-d) TEM, and (e, f) HAADF-STEM images of Cu/Ru@C-1b, showing the high dispersion of small Cu/Ru nanoparticles throughout the carbon structures. Inset in (a): SAED patterns showing crystalline nature of the Cu/Ru nanoparticles.

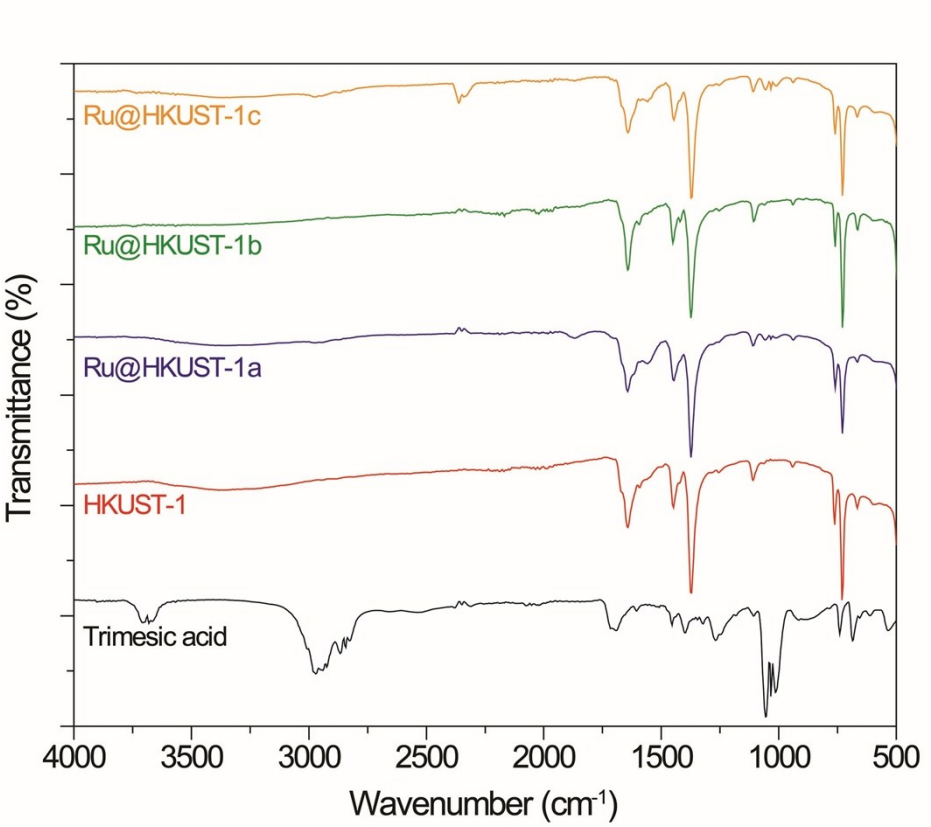

Fig. S5 Fourier transform infrared spectroscopy (FTIR) analyses of 1,3,5-benzene tricarboxylic acid (trimesic acid), HKUST-1, Ru@HKUST-1a, -1b and -1c.

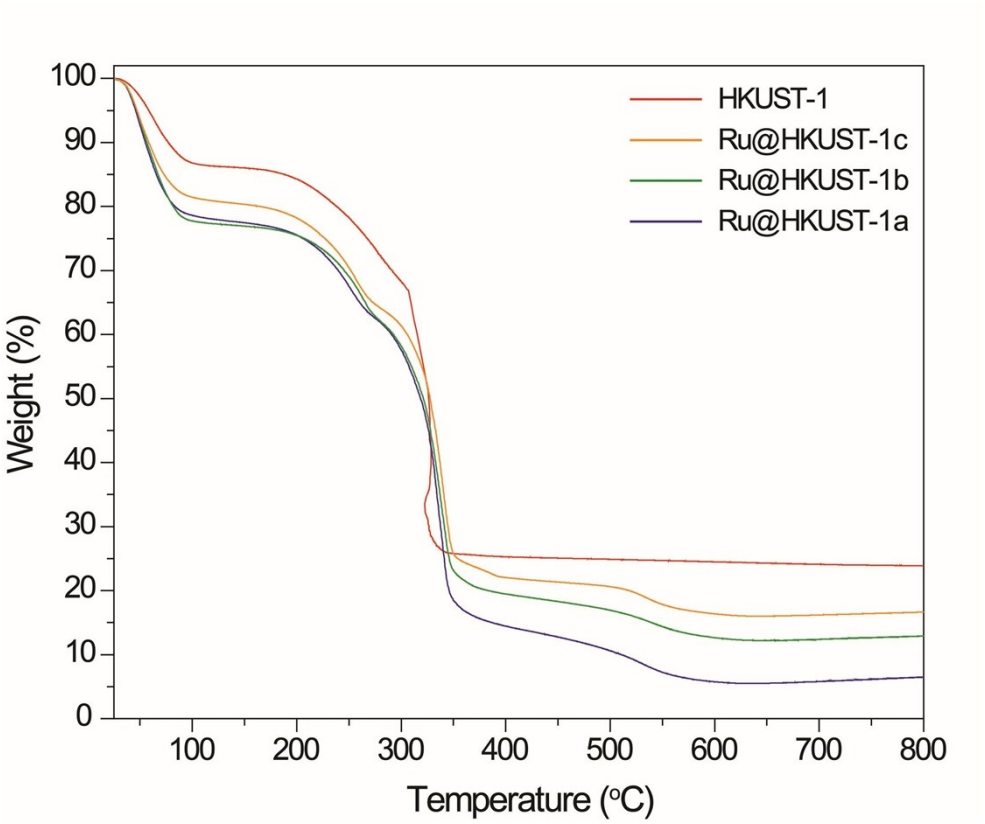

Fig. S6 TGA of HKUST-1, Ru@HKUST-1a, -1b and -1c under an argon atmosphere, showing the thermal stabilities up to 250 °C.

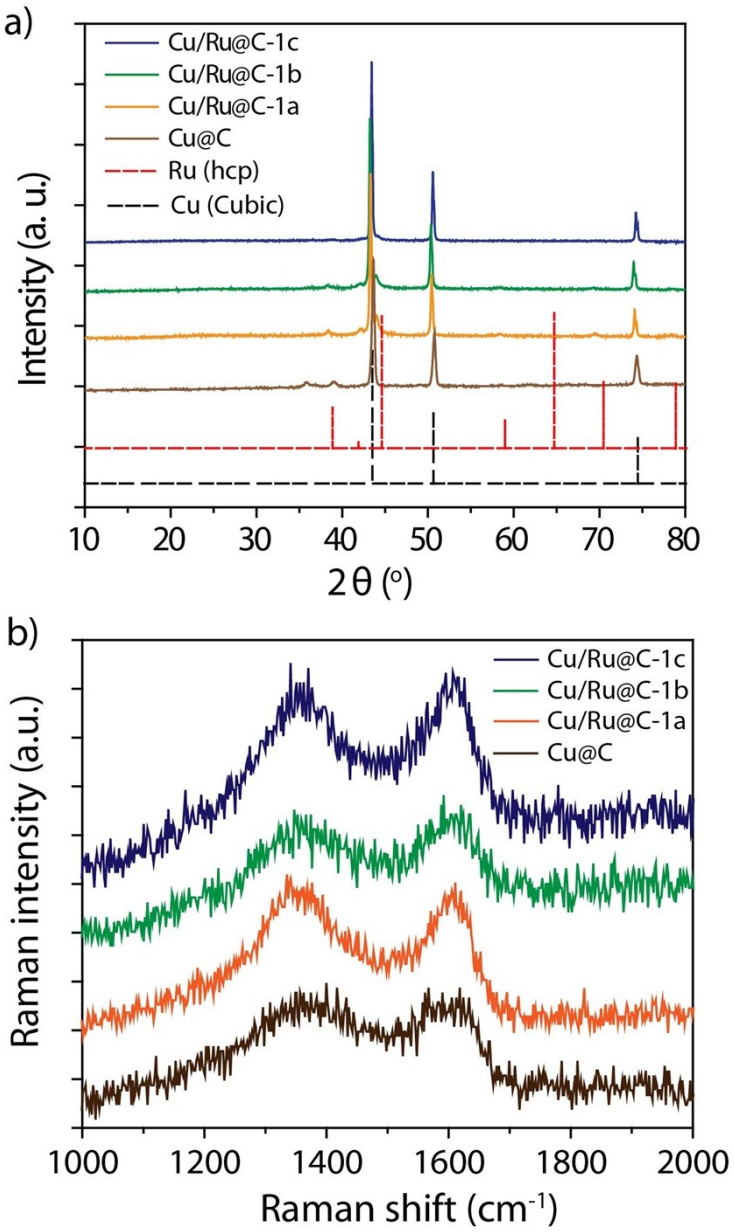

Fig. S7 (a) PXRD analyses of Cu@C, Cu/Ru@C-1a, -1b and -1c. The dotted black and red lines represent the simulated diffractions of Cu(cubic) and Ru(hcp) phases, respectively. (b) Raman spectra of Cu@C, Cu/Ru@C-1a, -1b and -1c, showing the I_D/I_G ratios of 1.00, 1.04, 0.97 and 0.96, respectively.

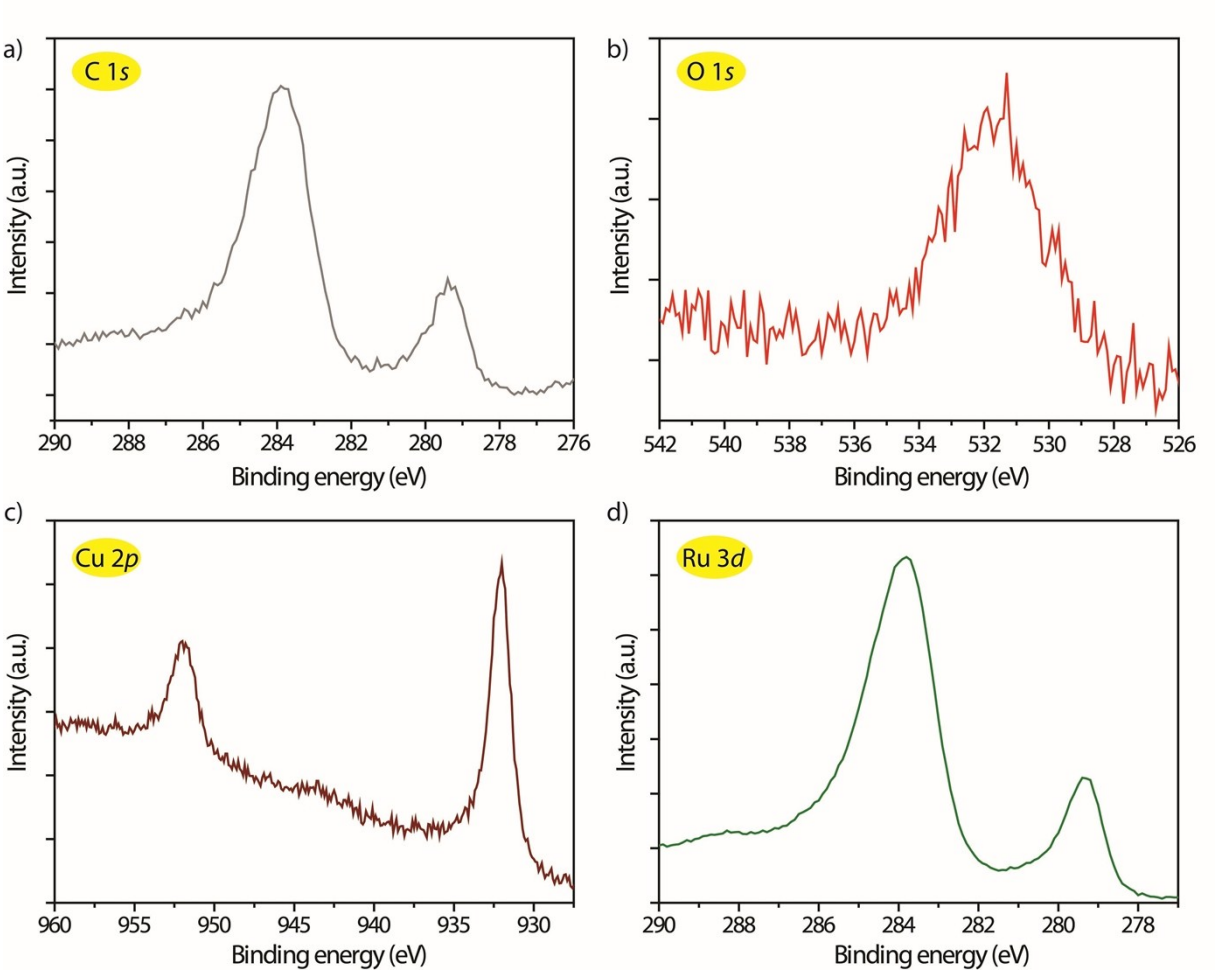

Fig. S8 XPS analyses of Cu/Ru@C-1b at (a) C 1*s* levels, (b) O 1*s* levels, (c) Cu 2*p* levels, and (d) Ru 3*d* levels, showing the presence of Cu and Ru metals in carbon matrix.

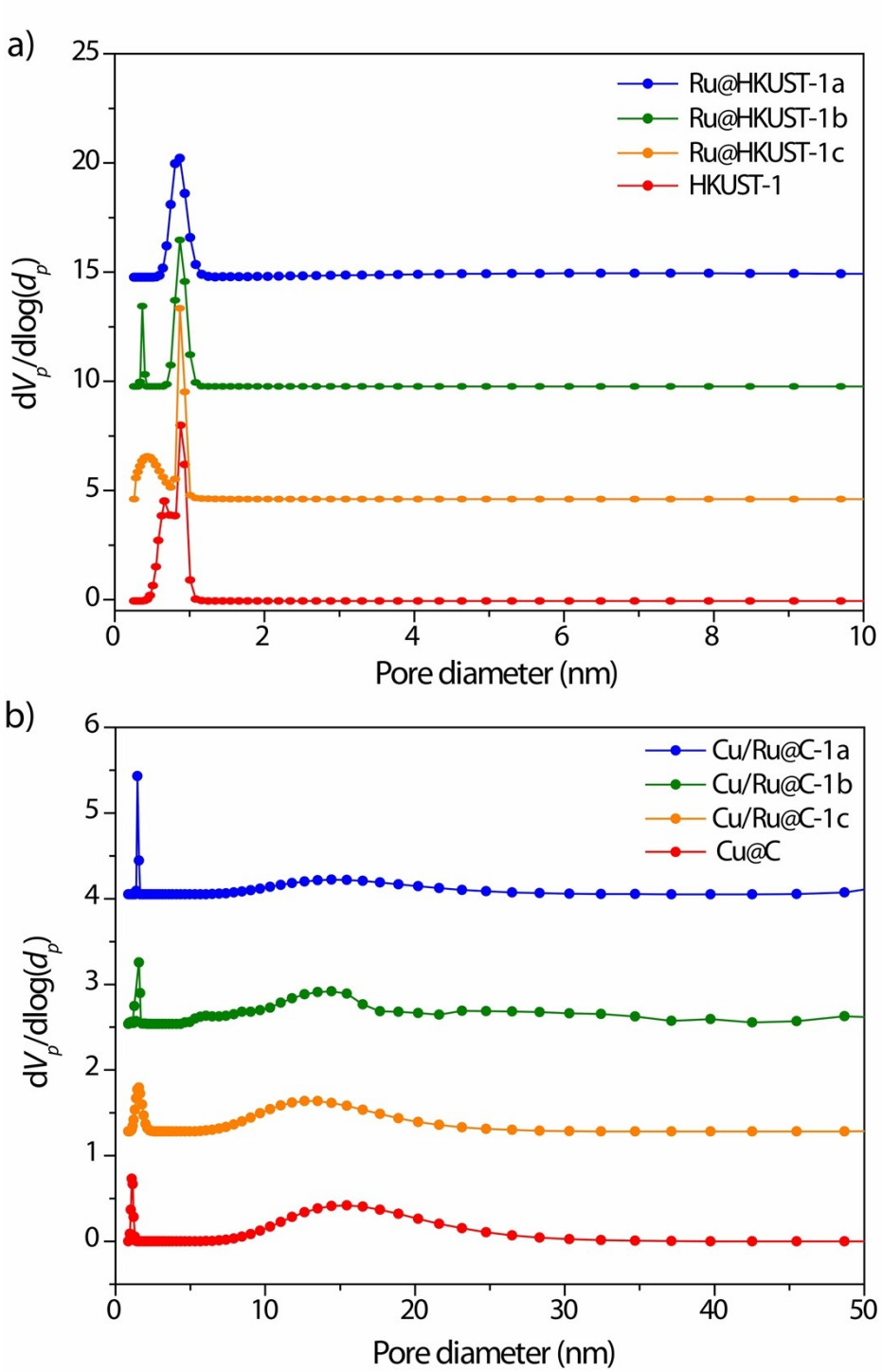

Fig. S9 Non-local density functional theory (NLDFT) pore size distributions for (a) HKUST-1, Ru@HKUST-1a, -1b and -1c, and (b) Cu@C, Cu/Ru@C-1a, -1b and -1c.

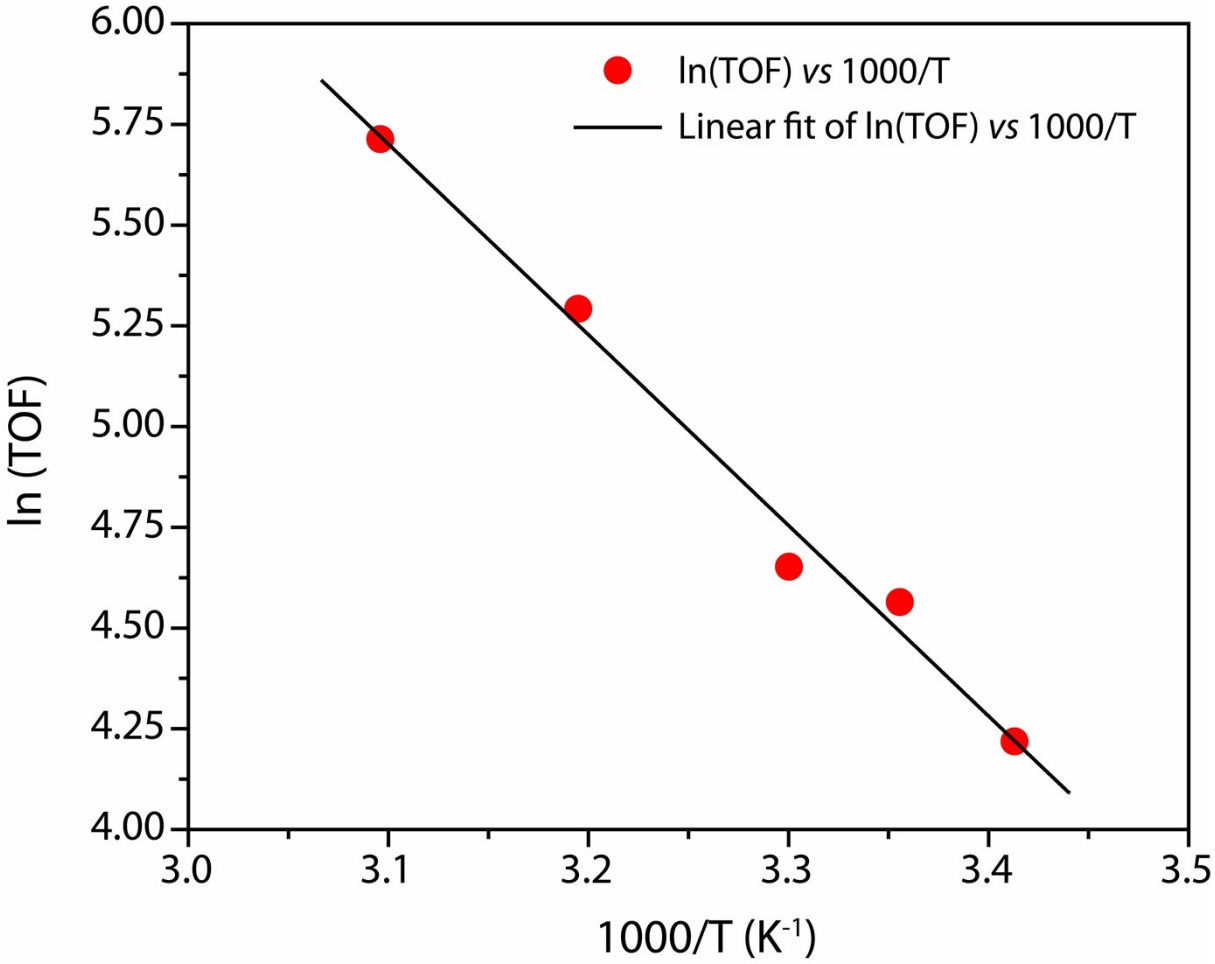

Fig. S10 Arrhenius plot (ln(TOF) *vs.* 1/T) for Cu/Ru@C-1b catalyst within the temperature range of 293−323 K, showing the activation energy (*E*a) of 39.2 kJ mol^{-1}.

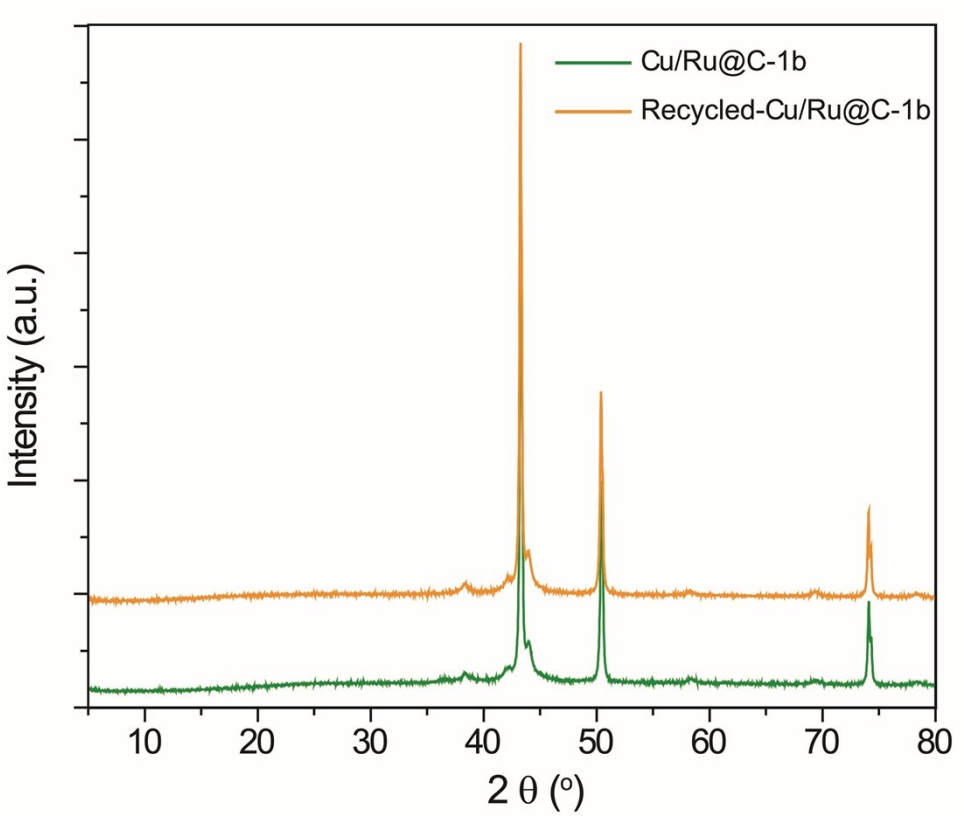

Fig. S11 PXRD analyses of Cu/Ru@C-1b after 5 cycles of ammonia borane hydrolysis, suggesting the maintenance of structure integrity during the catalytic reaction.

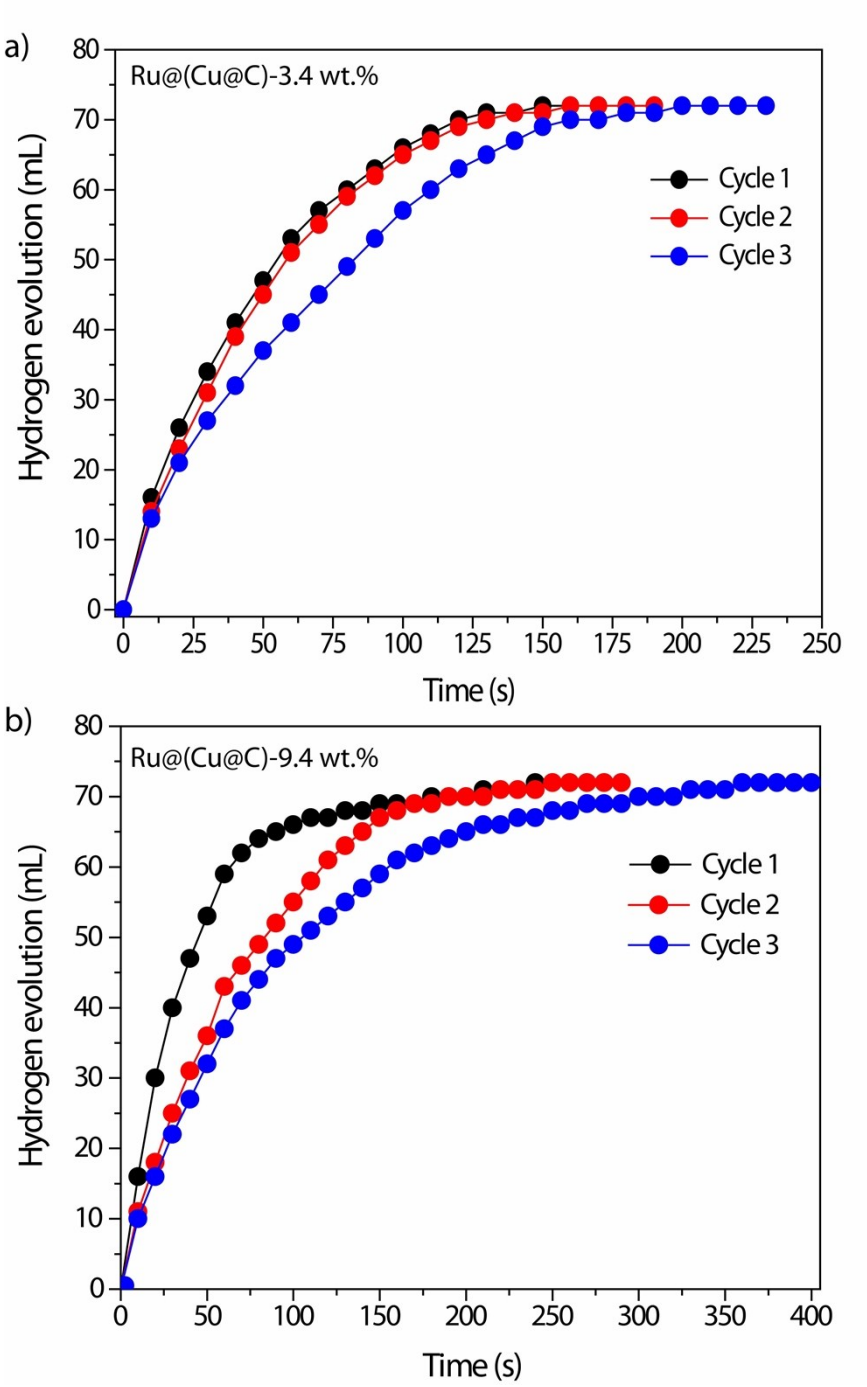

Fig. S12 Plot of time *vs.* volume of hydrogen generated from hydrolysis of AB (1 mmol) at 298 K catalyzed by (a) Ru@(Cu@C)-3.4 wt.%, and (b) Ru@(Cu@C)-9.4 wt.% catalysts for 3 catalytic cycles. The loss in catalytic performance with increasing number of cycles can be attributed to the aggregation of metal nanoparticles during the reaction.

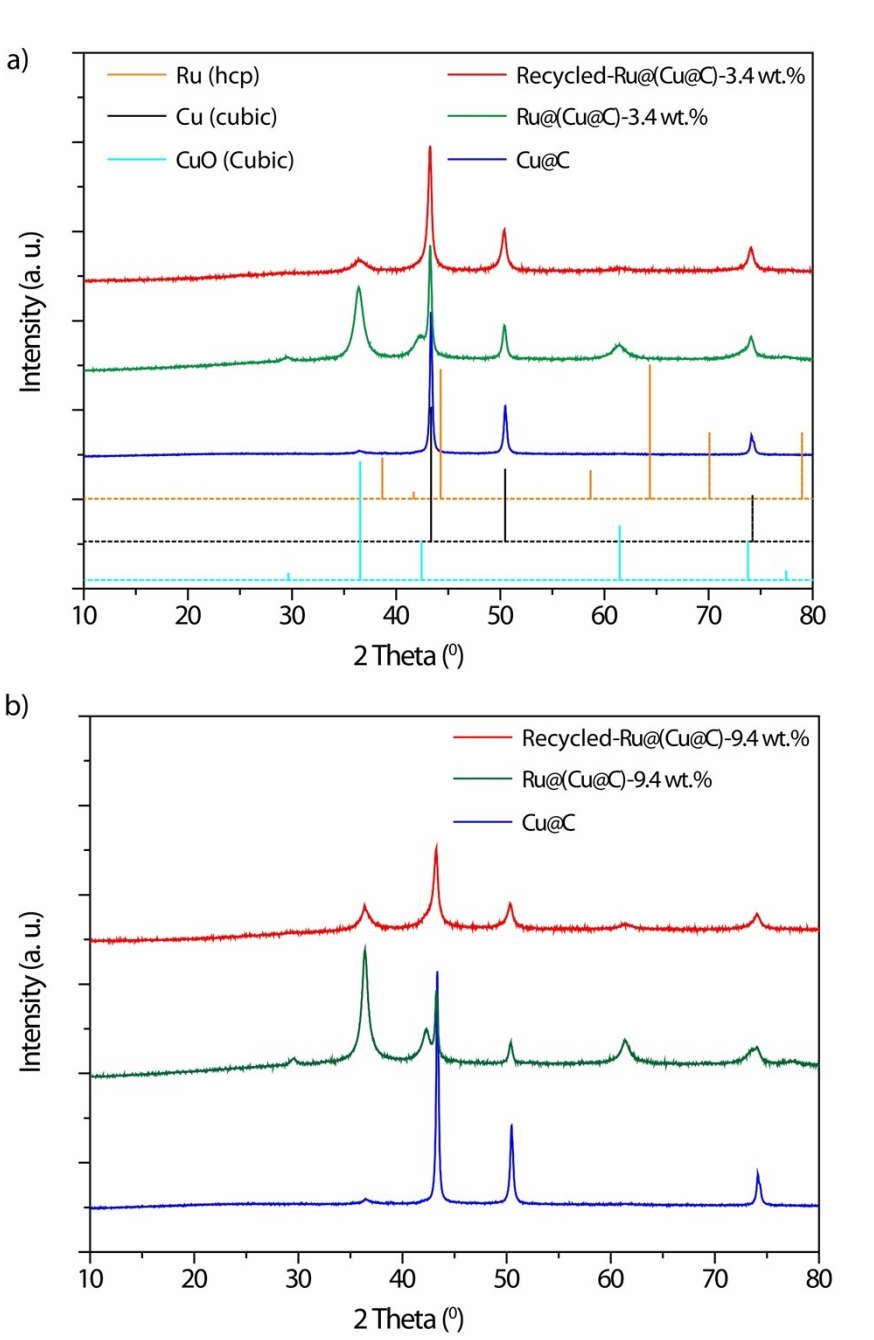

Fig. S13 PXRD analyses of (a) Cu@C, Ru@(Cu@C)-3.4 wt.% and recycled Ru@(Cu@C)-3.4 wt.%, and (b) Cu@C, Ru@(Cu@C)-9.4 wt.% and recycled Ru@(Cu@C)-9.4 wt.%.

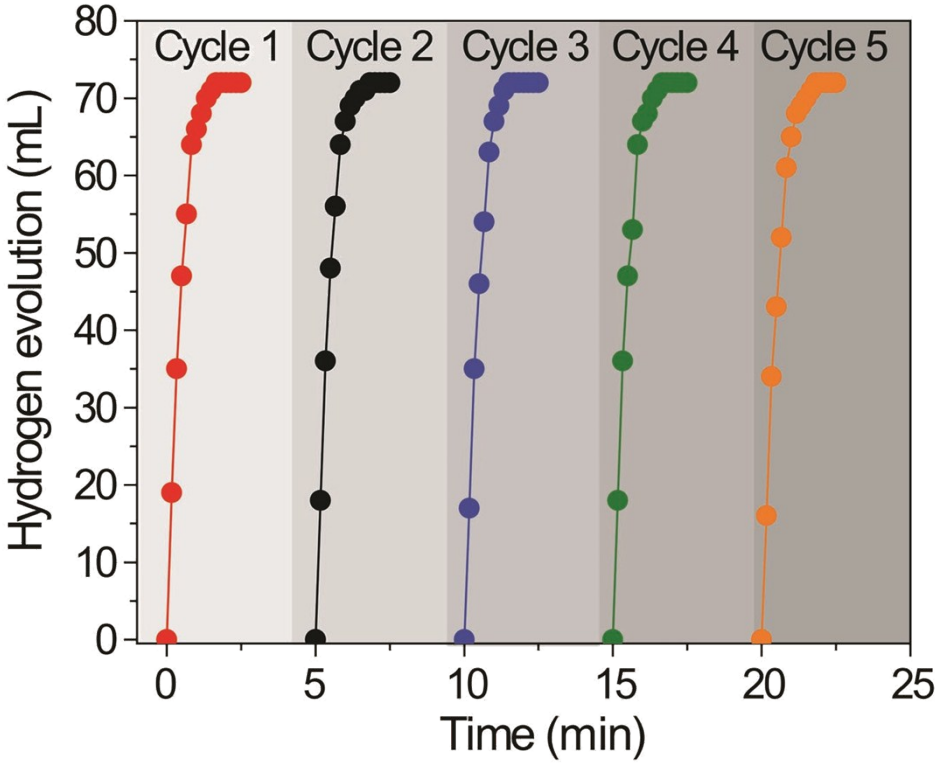

Fig. S14 Durability test for the hydrogen generation from aqueous AB solution catalyzed by Cu/Ru@C-1b. Additional aliquots of 1 mL AB solution (1.0 mmol) were added into the reaction flask after the completion of the last run.

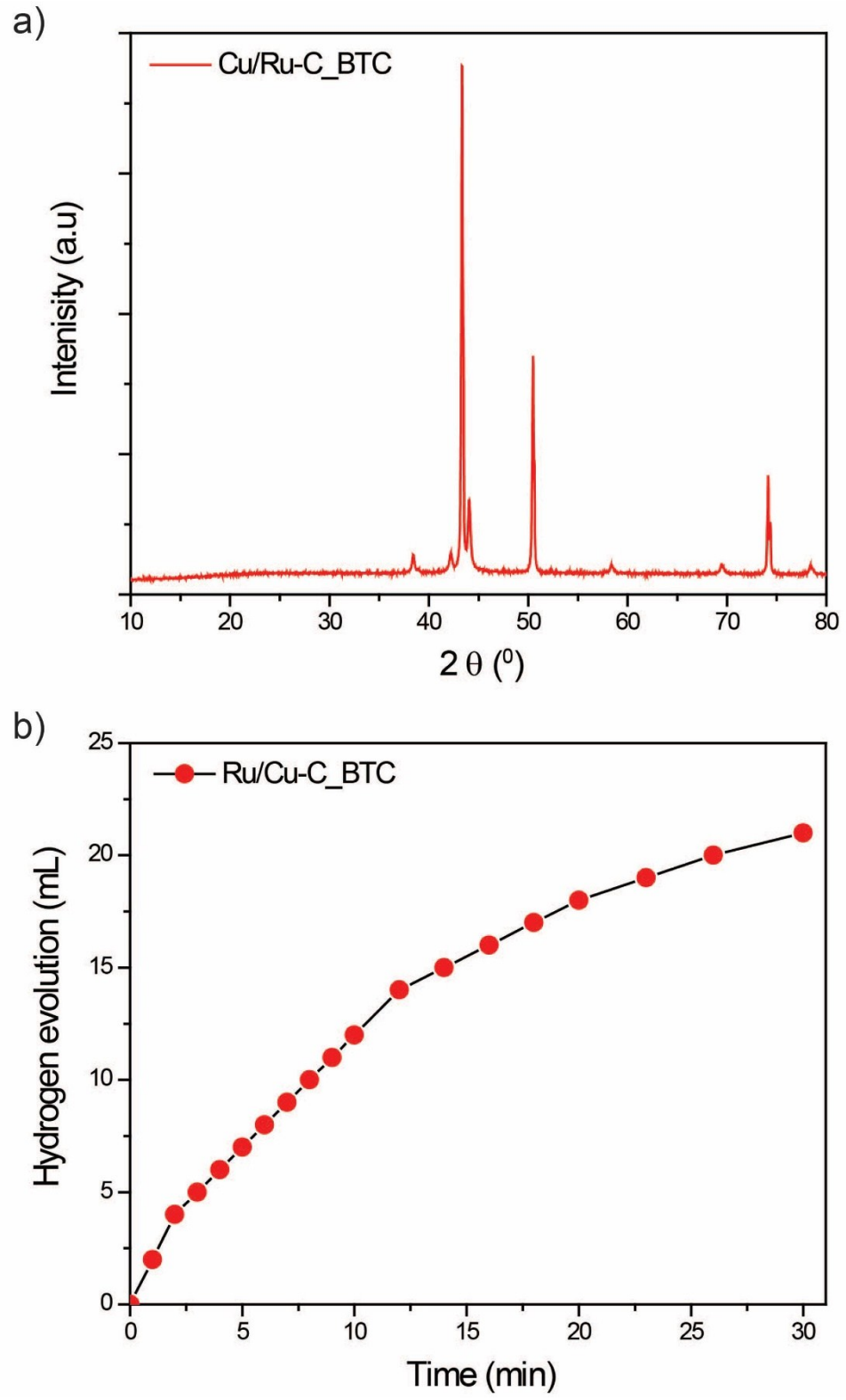

Fig. S15 (a) PXRD analysis of the carbonaceous material (Cu/Ru-C_BTC) obtained by the direct pyrolysis of starting materials ($RuCl_3.xH_2O$, $Cu(NO_3)_2.3H_2O$ and BTC linker) at 800 ^oC under argon atmosphere. (b) Plot of time *vs.* volume of hydrogen generated from hydrolysis of AB (1 mmol) at 298 K catalyzed by Cu/Ru-C_BTC, indicating a very low catalytic activity.

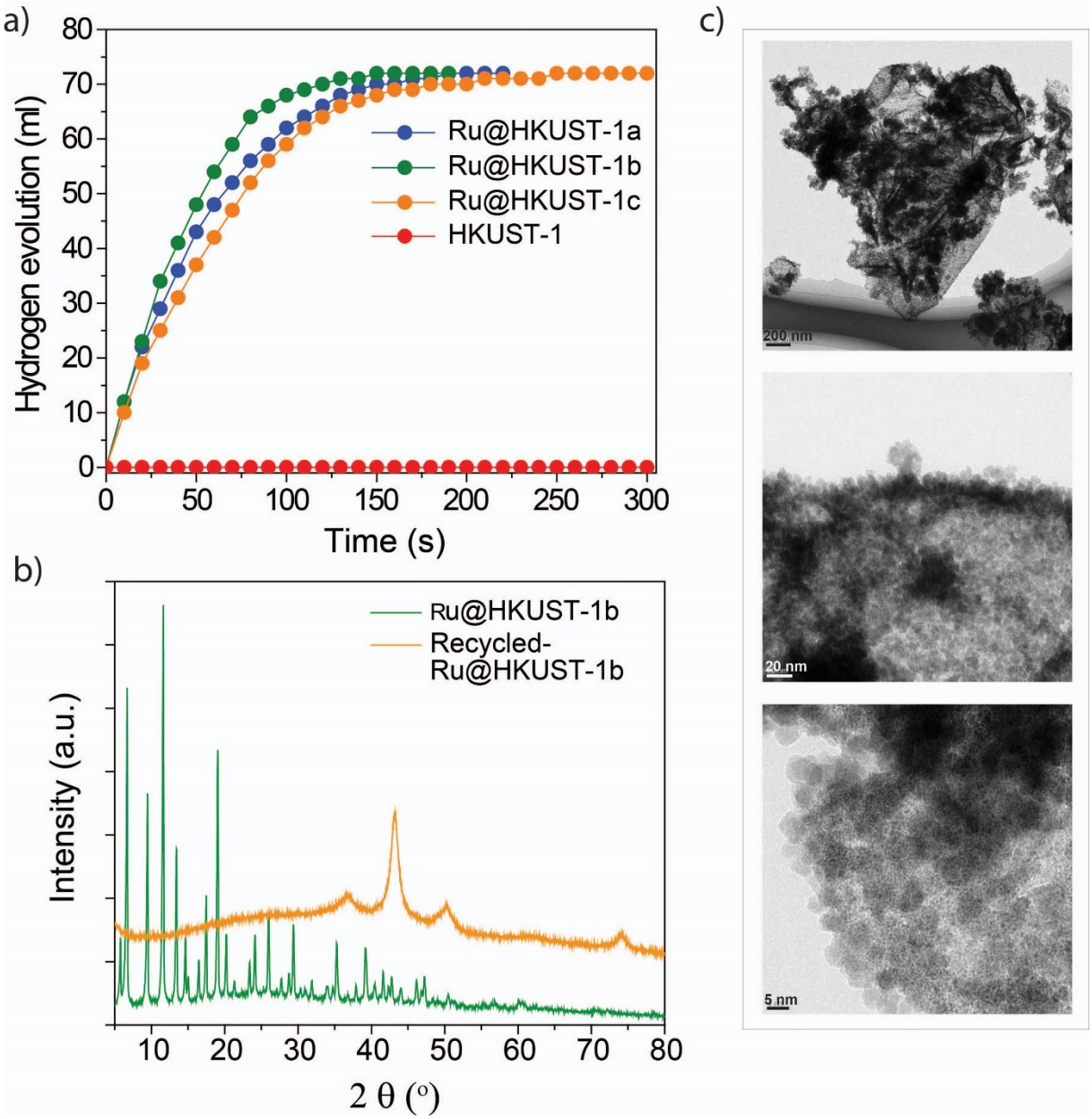

Fig. S16 (a) Plots of time *vs.* volume of hydrogen generated from hydrolysis of AB (1 mmol) at 298 K catalyzed by HKUST-1, Ru-HKUST-1a, -1b and -1c (50 mg). (b) PXRD analyses of Ru@HKUST-1b after ammonia borane treatment. The destruction of MOF frameworks during the ammonia borane treatment is clearly visible in PXRD patterns. (c) TEM images of recycled Ru-HKUST-1b after 1st cycle for hydrolysis of AB showing the complete destruction of original octahedron morphology.

Section S4. References

(1) Q.-L. Zhu, N. Tsumori and Q. Xu, *J. Am. Chem. Soc.* 2015, **137**, 11743−11748.